EPJ Web of Conferences **32**, 03002 (2012)
DOI: 10.1051/epjconf/20123203002

Visualization of core and edge MHD instabilities in 2D using ECEI

G.S. Yun, W. Lee, M.J. Choi, J. Lee, G.H. Choe, H.K. Park[1], C.W. Domier, N.C. Luhmann, Jr.[2], A. J. H. Donné[3], J.H. Lee, S.I. Park, M. Joung, Y.S. Bae, Y.M. Jeon, S.W. Yoon, and KSTAR team[4]

[1]POSTECH, Pohang 790-784, Republic of Korea
[2]University of California, Davis, CA 95616, U.S.A.
[3]Dutch Institute for Fundamental Energy Research, 3430 BE Nieuwegein, the Netherlands
[4]National Fusion Research Institute, Daejeon 305-333, Republic of Korea

Abstract. MHD instabilities in the core and edge of the KSTAR plasmas have been visualized in 2D using an electron cyclotron emission imaging (ECEI) system with sufficient time and space resolutions for the study of the underlying dynamics. In the core region where the ECE optical depth is large, the ECEI has provided localized measurements of fast MHD phenomena such as the crash of internal kinks and coalescence of dual flux tubes. In the edge pedestal region of H-mode plasmas where the optical depth is marginal, the ECEI measurements were found to be still localized and were able to provide detailed 2D images of edge localized modes (ELMs) such as the growth of multiple filamentary structures and the crash of the pedestal characterized by fast localized bursts of the filaments [3]. The effect of electron temperature and density fluctuations on the ECE signals has been analysed to understand the limitations of the edge ECEI measurements.

1 Introduction

Each flux surface of ideal tokamak plasma in equilibrium (Fig.1a) has uniform electron temperature (T_e) and density (n_e) owing to the fast heat and particle transport along the helical magnetic field lines constituting the flux surface. Thus, the equilibrium state is well described by 1D radial profiles, which are symmetric in the flux coordinates. Magnetohydrodynamic (MHD) instabilities can distort the flux surfaces, partly breaking the symmetry (Fig.1b). The conventional 1D radial profile diagnostics would be still sufficient if the MHD perturbation is helically symmetric, i.e., the perturbation amplitude is uniform along the (original unperturbed) field lines as illustrated in Fig.1c. However, 2D diagnostic imaging (Fig.1d) becomes necessary (at least advantageous) when the perturbation contains substantial helical asymmetry or the changes of the perturbation structure is too rapid to be reconstructed by the 1D profiles such as in sawtooth crashes.

Electron Cyclotron Emission Imaging (ECEI) is a passive microwave imaging technique for 2D measurement of local electron temperature (T_e) based on the established 1D ECE radiometry. The ECEI systems have been recently installed in systems in several tokamaks and made substantial contributions to the physics understanding of sawtooth instabilities [1], tearing modes [2], Alfvén eigenmodes [3], and edge localized modes (ELMs) [4]. In these studies, the extraordinary second

harmonic (X2) ECE radiations were measured and interpreted as local T_e measurements as usual [5], except two cases: (1) during the sawtooth crash phase where nonthermal electrons could be generated and enhance the ECE intensity or radiation temperature (T_{ECE}) above the thermal level (T_e) and (2) the edge pedestal region where the optical depth is marginal and decreases rapidly toward the separatrix.

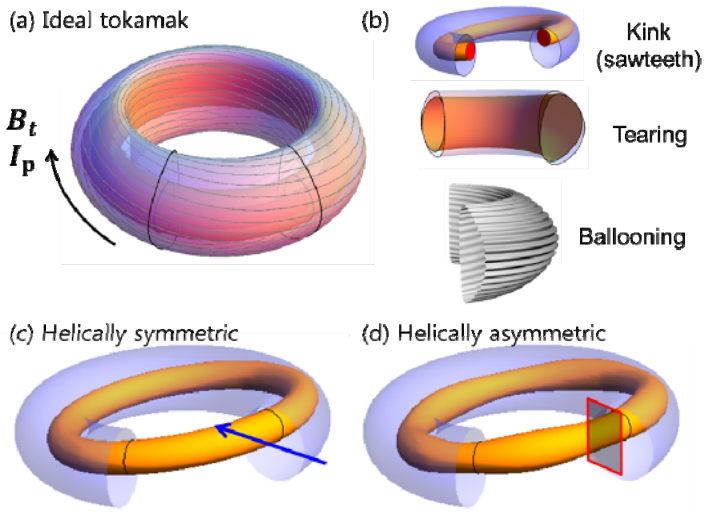

Figure 1 (a) Nested flux surfaces and helical field lines of an ideal tokamak. (b) Distortion of flux surfaces by MHD instabilities. (c) Helically symmetric internal kink. The arrow indicates the sight line of a 1D profile diagnostic. (d) Helically asymmetric internal link, whose structure may only be properly captured by 2D imaging diagnostic.

2 KSTAR ECEI

The KSTAR ECEI system [6] is schematically shown in Fig.2a. The operation frequency and radial ranges are illustrated in Fig.2b. The front optics optically delivers the ECE radiation onto a pair of independent heterodyne detector arrays. The lenses in the front optics, made of high density polyethylene (HDPE), provide flexible zooming and focusing like a camera lens [7]. Note that the radial detection range is determined by the frequency of the local oscillator (LO) and the optical focus is controlled to match the frequency focus in order to maximize the optical throughput. Combined with wideband LO sources (backward wave oscillators) and flexible optics, the ECEI system provides simultaneous measurement of two regions in the same poloidal crosssection as denoted by HFS (high-field side) and LFS (low-field side).

Each detector array box [8,9] has 24 vertically aligned Schottky diode detectors mounted onto wideband strip antennas, which are optimized for the detection of the vertically polarized X2 ECE in the W- and F-band microwave range (i.e., ~75—140 GHz). This corresponds to the 2nd harmonic ECE frequencies at B_0 = 2 T operation, the magnetic field at the major radius R_0 = 1.8 m. The array box downconverts the ECE microwave and amplifies the intermediate frequency (IF) signals, which are then delivered to the RF electronic modules. In each RF module [9], the IF signals (2.5—8.8 GHz) are split into 8 equally spaced frequency bands (0.7 GHz bandwidth), which corresponds to 8 different radial locations in the plasma. The radially resolved IF signals are integrated (video bandwidth ~ 400 kHz) and finally sampled by the digitizers (up to 2 MHz). The total number of channels is 24×8=192 with the spatial resolution ~ 1–2 cm and the time resolution ~ 1 μs.

For high field operations B_0 > 3 T, the X2 ECE exceeds the detectable range. In order to extend the operation range without replacing the detector arrays, the imaging of the fundamental ordinary

(O1) ECE has also been demonstrated at higher magnetic fields (B_0 >= 3T) using a large-aperture quarter wave plate [10], which rotates the parallel polarized O1 wave into a vertically polarized wave.

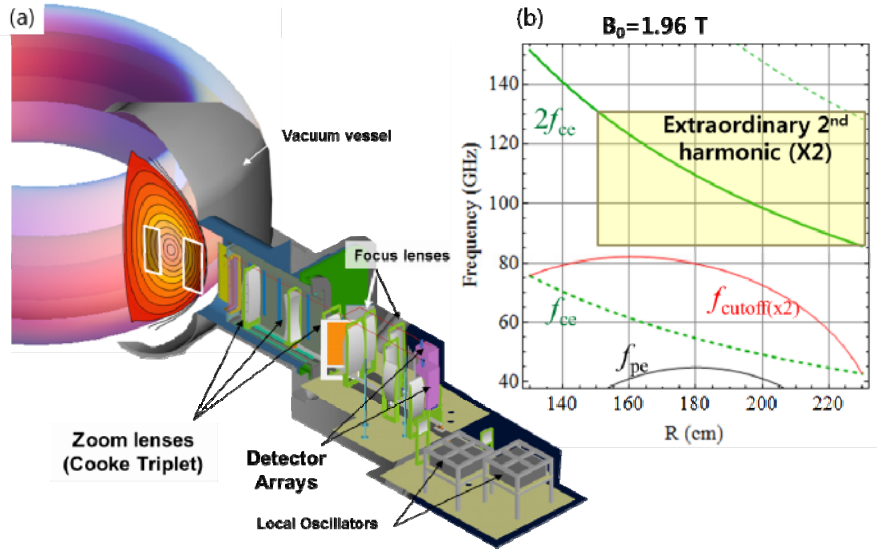

Figure 2 (a) KSTAR ECEI system. The two highlighted regions in the poloidal crosssection correspond to the sight areas of individual array boxes. (b) The range of the ECEI operation in the frequency and radial position domain. f_{ce} denotes the cold resonance cyclotron frequency. f_{pe} is the plasma frequency and f_{cutoff} is the cutoff frequency for X2 ECE waves.

3 Summary of KSTAR ECEI results

The KSTAR ECEI system has been used to study various MHD instabilities in the core and edge, including sawteeth, tearing modes, and edge localized modes. In the following example images of MHD instabilities, it is important to note that the apparent poloidal rotation (V^*_{pol}) of the instability structure (or mode) in the ECEI view at a fixed toroidal location is a combined effect of the plasma toroidal rotation (V_{tor}), the true poloidal flow (V_{pol}), the phase velocity (V_{ph}) of the instability mode as illustrated by Fig.3: $V^*_{pol} = V_{pol} - V_{tor} \times \tan\alpha + V_{ph}$, where α is the pitch angle of the instability.

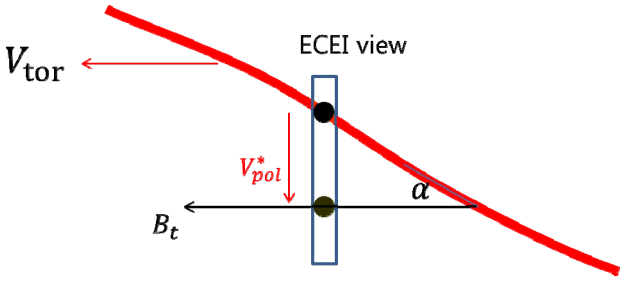

Figure 3 Apparent poloidal rotation (V^*_{pol}) of an MHD instability structure. The plasma toroidal rotation (V_{tor}) is from right to left. The finite pitch angle α makes the toroidal rotation appears as a downward poloidal rotation in the ECEI view.

(1) The KSTAR ECEI system has been routinely operated for simultaneous 2D visualization of core and edge MHD instabilities to study the interaction between them. The following example shows the internal kink and edge-localized modes (ELMs) [4].

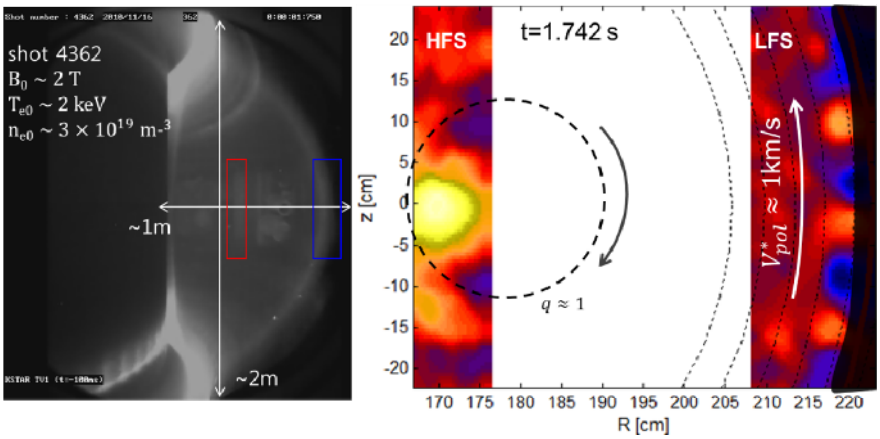

Figure 4 (Left) Visible TV image of the ELM-ing H-mode discharge (shot 4362). The red and blue rectangles indicate the HFS and LFS views of the ECEI system, respectively. (Right) Simultaneous imaging of the internal kink in the core and the ELM filaments in the edge.

(2) The ELM crash dynamics has been studied in detail, revealing that the crash is typically consisted of multiple bursts of ELM filaments [4]. Each burst is both poloidally and toroidally localized (Fig. 5).

(3) Alterations of ELM structure and dynamics caused by n=1 magnetic perturbations (MPs) [11] and supersonic molecular beam injection (SMBI) [12] have been measured to study the mechanisms of ELM suppression and mitigation (Fig. 6)

(4) Various modified sawtooth structures different from the normal internal kink [13, 14] have been found under electron cyclotron resonance heating (ECRH) conditions (Fig. 7), shedding a new light on the sawtooth control mechanism.

(5) *m/n* = 2/1 and 3/2 tearing modes have been observed in plasmas with n=1 resonant MPs [15]. The effect of MPs on the tearing instability is being investigated (Fig. 8).

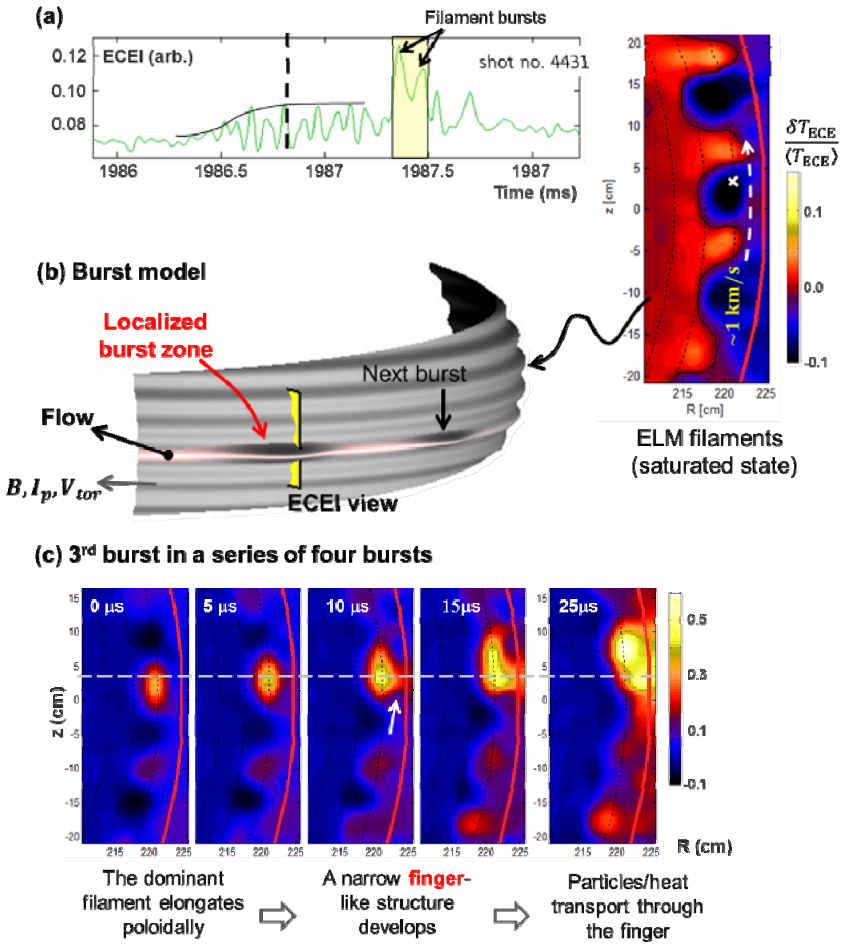

Figure 5 (a) Time trace of an ECEI channel at the pedestal position indicated by an arrow in the right figure (shot no. 4431), which corresponds to the saturated state of the ELM filaments. (b) A phenomenological model for the ELM crash consisted of localized multiple bursts of filaments. (c) A sequence of frames showing the process of the filament burst.

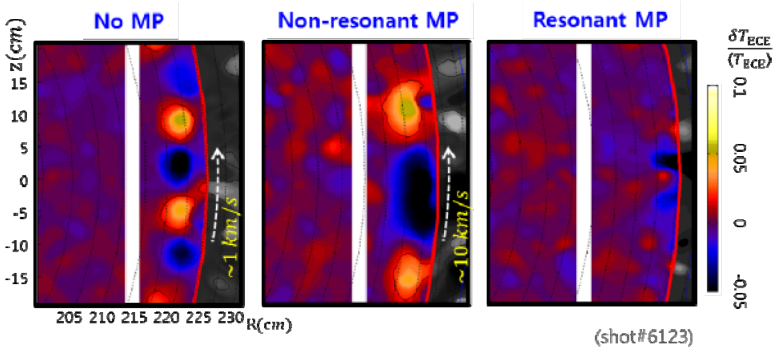

Figure 6 Alteration of the ELM filament structure under n=1 external MPs (shot no.6123). The second image corresponds to the ELM intensification by a non-resonant MP and the last image corresponds to the ELM suppressed phase by a resonant MP.

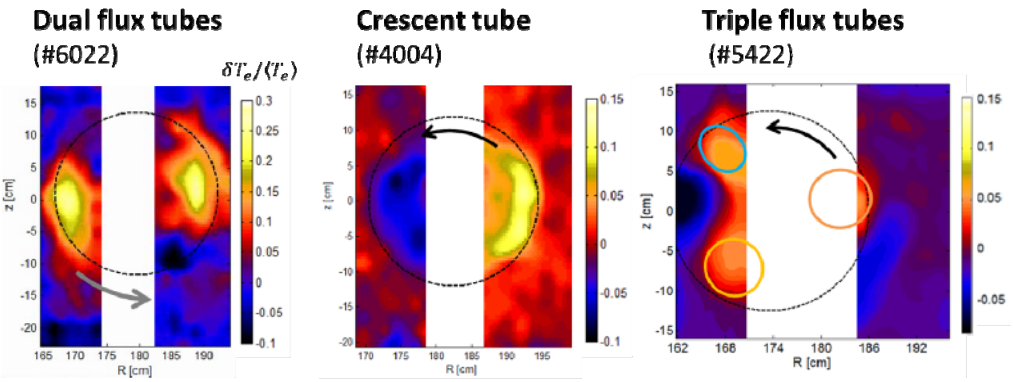

Figure 7 Modified sawtooth structures under ECRH. Dashed circles are the approximate q=1 surface.

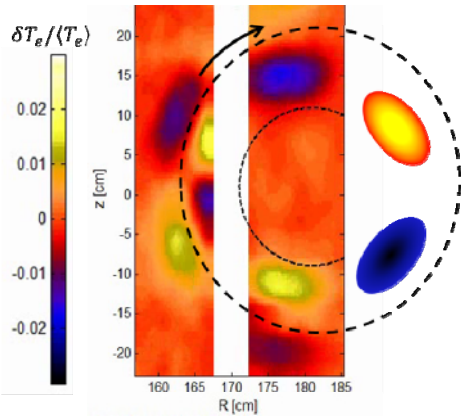

Figure 8 *m/n* = 3/2 tearing mode observed when the *n*=1 resonant MP was applied (shot no. 6304, t=4.483s).

4 Discussion on the edge ECE images

The interpretation of the ECEI images of the ELM filaments is not straightforward due to the marginal optical thickness in the pedestal region. The critical questions are whether the ELM filament images are localized measurements and whether the ECE intensity at the filament region depends on T_e only or not.

The short answer to the first question is positive, which is based on the estimation of the optical depth profile and the observed coherent rotation of the filament structure. The following two-step argument has been used to prove that the observed filament structure is real. (1) The ECE is a local measurement at least for the left side of the filaments (i.e. radially inward) since the optical depth is sufficiently greater than 1 in that region. (2) The rotation of the filaments is coherent, which implies that the ECE is a local measurement for the rest of the filament region. The calculation of the emission profiles using the analytic formula by Bornatici [5] the shows that the ECE is indeed localized near the pedestal top.

The answer to the second question is negative. The radiative transfer equation in the slab geometry indicates that the density fluctuation (δn_e) effect could be substantial on the ECE intensity (T_{ECE}) of the ELM filaments, $\frac{\delta T_{ECE}}{\langle T_{ECE} \rangle} \approx \{1 + A(\tau)\}\frac{\delta T_e}{\langle T_e \rangle} + A(\tau)\frac{\delta n_e}{\langle n_e \rangle}$, where A(τ) is a function of the optical depth τ [16]. The contributions of δn_e and δT_e on T_{ECE} are unknown at present

due to the lack of the edge profile diagnostics. A simultaneous 2D measurement of X2 and O1 waves [10] is planned to resolve the effects of δn_e and δT_e utilizing the large difference in the optical depths or A(τ) between X2 and O1 (see Fig.9).

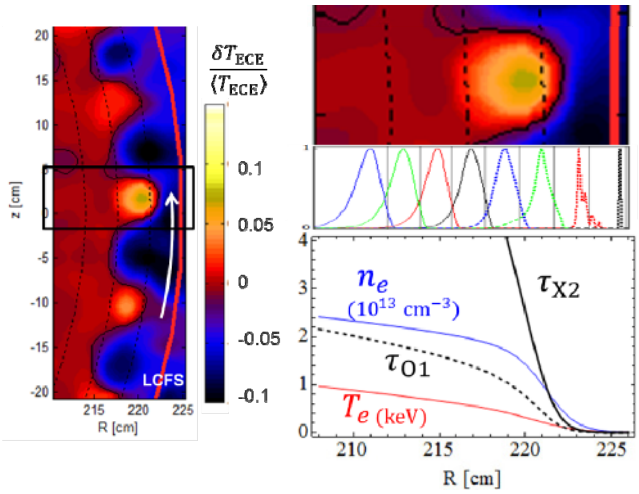

Figure 9 Optical depth profile across the ELM filaments (right bottom). The optical depth for O1 ECE (τ_{O1}) is also shown for comparison. The middle figure on the right is the normalized X2 emission profiles of individual ECEI channels, showing that the ECE is radially localized in the filament region.

References

1. H.K. Park et al., Phys. Rev. Lett. **96**, 195003 (2006)
2. I.G. J. Classen et al., Phys. Rev. Lett. **98**, 035001 (2007)
3. B.J. Tobias et al., Phys. Rev. Lett. **106**, 075003 (2011)
4. G.S. Yun et al., Phys. Rev. Lett. **107**, 045004 (2011)
5. M. Bornatici, R. Cano, O. De Barbieri, and F. Engelmann, Nucl. Fusion **23**, 1153 (1983)
6. G. S. Yun et al., Rev. Sci. Instrum. **81**, 10D930 (2010)
7. T. Liang et al., Rev. Sci. Instrum. **81**, 10D909 (2010)
8. B. Tobias et al., Rev. Sci. Instrum. **81**, 10D928 (2010)
9. C. Domier et al., Rev. Sci. Instrum. **77**, 10E924(2006)
10. J. Lee et al., J. Instrum. **7**, C01037 (2012)
11. G.S. Yun et al., Phys. Plasmas **19**, 056114 (2012).
12. W.W. Xiao et al., KSTAR Conference, Muju, Korea (2012)
13. G.S. Yun et al., 53rd APS DPP Conference, Salt Lake City, Utah, USA (2011)
14. G.H. Choe et al., KSTAR Conference, Muju, Korea (2012)
15. M.J. Choi et al., KSTAR Conference, Muju, Korea (2012)
16. G.S. Yun et al., J. Instrum. **7**, C01024 (2012)